3D structure of the Milky Way out to 10 kpc from the Sun

Catalogue of large molecular clouds in the Galactic Plane

Sara Rezaei Kh.[1,2], Henrik Beuther[1], Robert A. Benjamin[3], Anna-Christina Eilers[4], Thomas Henning[1], Maria J. Jiménez-Donaire[6,7], and Marc-Antoine Miville-Deschênes[5]

[1] Max-Planck-Institute for Astronomy, Königstuhl 17, 69117 Heidelberg, Germany
e-mail: `s.rezaei.kh@gmail.com`

[2] Chalmers University of Technology, Department of Space, Earth and Environment, SE-412 93 Gothenburg, Sweden
[3] Department of Physics, University of Wisconsin-Whitewater, Whitewater, WI 53190, USA
[4] Physics Department and Kavli Institute for Astrophysics and Space Research, Massachusetts Institute of Technology, 77 Massachusetts Ave, Cambridge MA 02139, USA
[5] Institut d'Astrophysique Spatiale, CNRS, Univ. Paris-Sud, Université Paris-Saclay, Bât. 121, F-91405 Orsay, France
[6] Observatorio Astronómico Nacional (IGN), C/Alfonso XII 3, 28014 Madrid, Spain
[7] Centro de Desarrollos Tecnológicos, Observatorio de Yebes (IGN), 19141 Yebes, Guadalajara, Spain

Received ——; accepted ——

Reporter: Lin Zhang（张琳）

Dec 1, 2024

Outline

- Introduction
- Data and methods
- Results
- Discussion
- Conclusion remarks

Introduction

Star-forming regions contribute to the overall evolution of galaxies and different galactic environments affect the formation and evolution of star-forming regions. The structures of the galactic disc components, such as spiral arms, influence the distribution and evolution of gas and dust, and therefore star formation in a galaxy.

Spiral galaxies exhibit active star formation within their spiral arms composed of a concentration of gas and dust. To understand the role of spiral arms in star and galaxy formation and evolution, knowledge of the location of the arms, as well as their components is of utmost value.

Numerous works have focused on characterising the positions of spiral arms in the Milky Way via various approaches; from studying young stars (Russeil 2003; CantatGaudin et al. 2018; Romero-Gómez et al. 2019), to atomic and molecular gas kinematics (Drimmel & Spergel 2001; Kalberla & Kerp 2009; Dame et al. 2001; Roman-Duval et al. 2010; MivilleDeschênes et al. 2017), and maser parallax measurements (Reid et al. 2019).

Introduction

However, despite all improvements, due to challenges in estimating distances and obscuration caused by line-of-sight (LOS) extinction, an accurate picture of the exact structure of our galaxy remains elusive to this date.

Since Gaia's launch in 2013, the Gaia satellite therefore offers an ideal set of data for studying nearby individual molecular cloud substructures in 3D (e.g. Großschedl et al. 2018; Rezaei Kh. et al. 2018a, 2020; Rezaei Kh. & Kainulainen 2022; Zucker et al. 2021), as well as the 3D structure of the local Milky Way (e.g. Green et al. 2019a; Leike et al. 2020; Vergely et al. 2022; Edenhofer et al. 2023).

However, due to the optical nature of the Gaia observations, the studies remain limited to nearby (< ~3 kpc) regions. Therefore, to study the large-scale physics of the ISM, complementary near-infrared (IR) datasets are of great importance.

In this work, we showcase the power of near-IR data combined with machine learning techniques to provide a novel 3D map of our Galaxy that expands out to 10 kpc.

Data and methods

- **2.1. 3D mapping technique** **(Rezaei Kh. et al. 2017, 2018b, 2020)**

  Input data: the 3D positions of the stars (l, b, d) and their LOS extinction.

  Likelihood: It then divides the LOS of each star into small 1D cells in order to approximate the observed extinction toward each star as the sum of the dust in each cell along its LOS.

  Prior: The model then takes into account the neighbouring correlation between all points in 3D using the Gaussian Process; i.e. the closer two points in the 3D space, the more correlated they are.

  Having prepared both the Likelihood and the Prior, the model uses extensive linear algebraic analysis to determine the probability distribution of dust density at any arbitrary point in the observed space, even along the LOS that was not originally observed.

Data and methods

The model incorporates several hyper-parameters determined by the input data (see Rezaei Kh. et al. 2017, 2018b, for more details).

a) One of these parameters is the cell size, which is tuned based on the typical spacing between input stars and serves as the minimum resolution for the final map. In areas with denser and more informative data, the map's resolution will be higher.

b) Another parameter is the correlation length, which defines the range over which spatial correlations exist. Typically, it is a few times the cell size to ensure the connection between nearby cells in 3D.

c) The third hyperparameter, known as the scale variance, is calculated using the data's amplitude and uncertainties, reflecting the variance of predictions. After introducing the datasets in the following section, we will detail these parameters for our models.

Data and methods

- **2.2. Input data: Distance and Extinction estimates**

The 16th data release of APOGEE published in 2020 (Jönsson et al. 2020), covers different parts of the Galactic plane out to distances beyond the Galactic centre and includes sources from the southern hemisphere (Jönsson et al. 2020).

Extinction measurements come directly from the APOGEE pipeline: all APOGEE sources have corresponding observations in multi-band photometry in the near- and mid-IR with the 2MASS and the WISE, respectively. Therefore their extinctions are easily estimated using the Rayleigh-Jeans Colour Excess Method (RJCE, Majewski et al. 2011).

The distance estimates for the APOGEE sources are calculated using spectrophotometric parallaxes computed based on the method of Hogg et al. (2019). The approach leverages a data-driven model that combines photometric and spectroscopic data, aiming to describe the parallaxes of giant stars. The study achieves a median relative uncertainty in spectrophotometric parallax of ~ 8%,

Data and methods

Given our specific interest in the structure of the Galactic Plane, and considering that the majority of APOGEE observations are designed for these regions.

a) only absolute Galactic heights below 1 kpc.

b) confining our map to the 10 kpc range along the X- and Y- axes.

Final sample: more than 44 000 stars.

We also note that the number of stars drops significantly in the inner ~500 pc, therefore we limit our predictions to distances beyond 1 kpc.

For the APOGEE data used in this work, the hyper-parameters are as follows:

cell size: 200 pc

correlation length: 1 kpc

scale variance: $5e-09\ pc^{-2}$

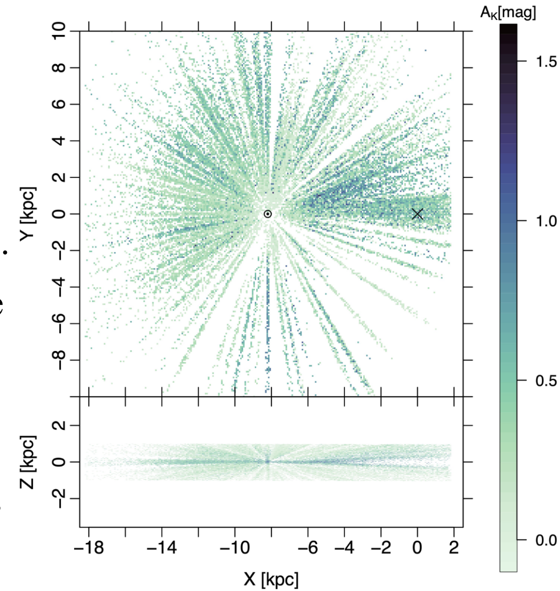

Fig. 1: Final sample used as our input data. The top panel shows the X-Y plane, perpendicular to the Galactic plane and the bottom panel presents the X-Z plane where our cut on the 1kpc Galactic height is visible. The colour shows estimated extinctions for individual stars. The Sun is at (-8.2,0,0) and the Galactic Centre is marked with an X, assuming the Sun is at the distance of 8.2 kpc from the Galactic Centre. The gaps between different LOS indicate that the sky is not observed uniformly by APOGEE.

Results

- **3.1. Features of the map**

We produce the 3D map of the dust in the Galactic plane for a radius of 10 kpc in X-Y plane and 750 pc in the Z direction. The densest structures of the map appears at a Galactocentric radius of about 4 kpc, likely associated with the so called Molecular Ring (Krumholz & McKee 2005).

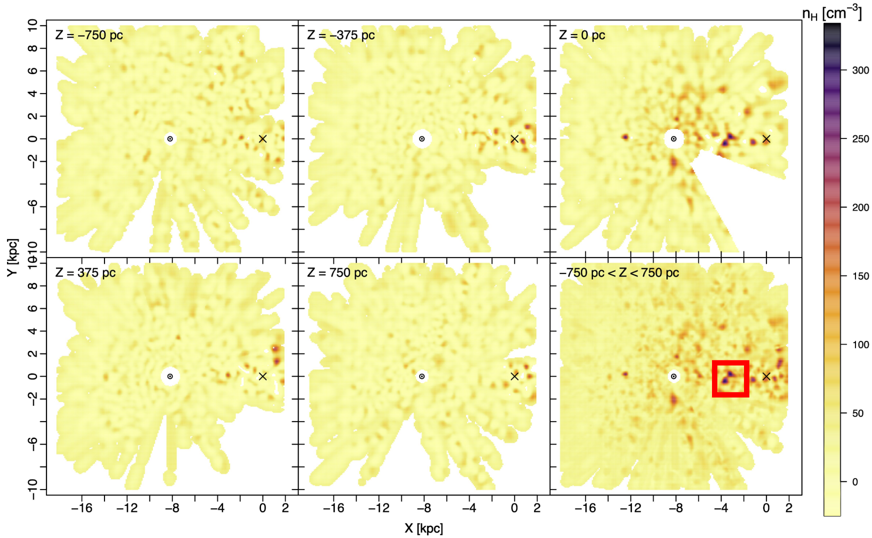

Fig. 2: Face-on view of our 3D map of the dust in the Galactic plane for different Galactic heights. The bottom right panel shows the combined map from -750 pc to 750 pc in the Galactic height. The colour shows the mean of our predicted density (cm^{-3}) for each pixel (100×100 in X-Y plane) in all panels except for the bottom right where the colour represents the maximum density within the 1.5 kpc height. The Sun is at (-8.2,0,0) and the Galactic Centre is marked with a ×, assuming the Sun is at the distance of 8.2 kpc

Results

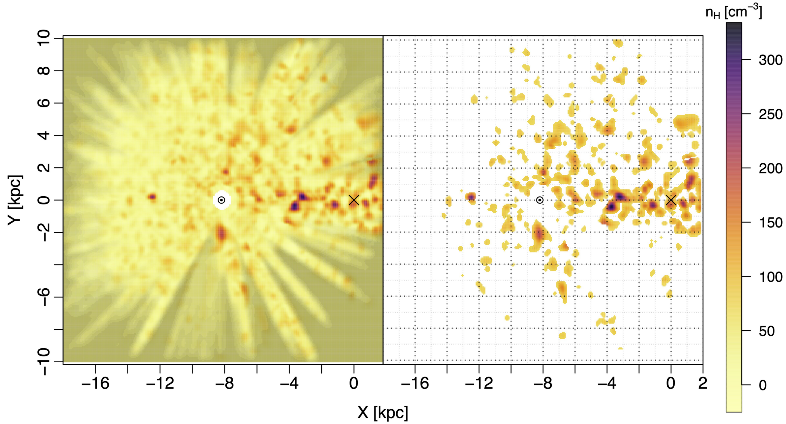

Fig. 3: Face-on view of the 3D map for all Galactic heights. Left panel: same as the bottom right panel of Fig. 2, in addition to having shaded areas illustrating regions of high uncertainty (fractional uncertainties larger than 50%). Right panel: clouds selected from the 3D map whose density values lie three standard deviations above the mean of the Gaussian Process. This corresponds to densities above 80 cm^{-3}.

The right panel of Fig. 3 shows clouds extracted from the 3D map with statistically significant densities. Statistically significant in this context means three standard deviations above the mean of the Gaussian process that is used for density calculations.

We go three standard deviations above the mean density of the Gaussian Process to have a pure sample of dense clouds. This corresponds to densities above ~$80cm^{-3}$. The fractional uncertainties of the selected clouds are between 5 and 30 percent. We select regions with densities above $100cm^{-3}$, corresponding to the molecular phase.

Results

One clear feature of the map is the presence of large cavities.

While we were able to extract a clear sample of clouds with reliable densities from the map, differentiating real cavities from regions of underestimated densities due to missing data is very difficult.

As a result, we limit our sample of the cavities to nearby regions (within ~ 4 kpc from the Sun) to avoid mistakenly categorizing regions without complete input data as cavities.

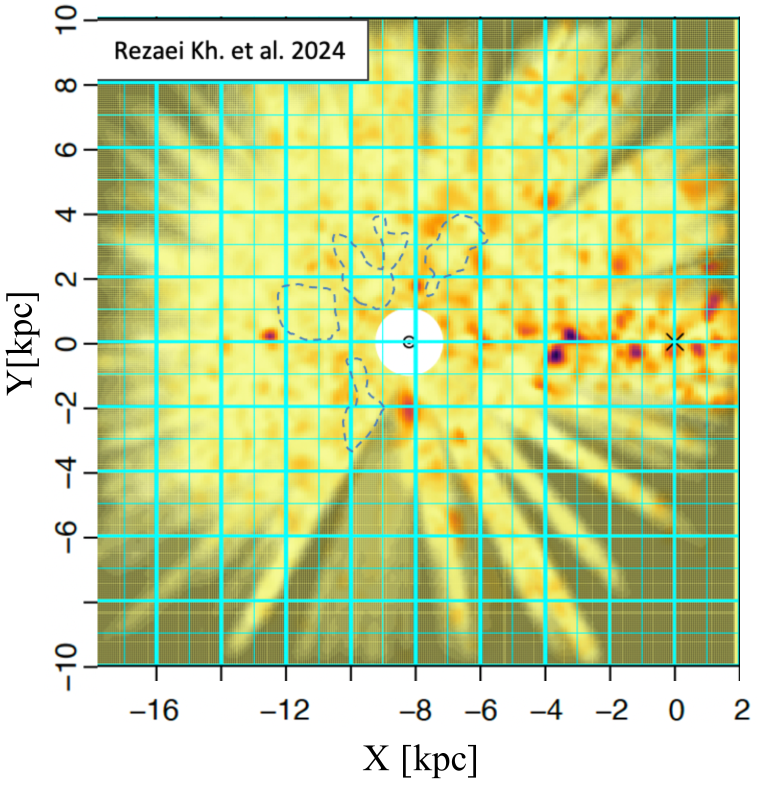

Results

- **3.2. Comparison to other 3D maps**

  Vergely et al. (2022): combining Gaia parallaxes with the crossmatch of the Gaia data with 2MASS and WISE photometry.

  Green et al. (2019b): multiband photometry from PANSTARRS together with the Gaia parallaxes to simultaneously derive distance and extinction to individual stars.

  Marshall et al. (2006): they measure the colour excess of stars by assuming a Galaxy model and the intrinsic colours of stars. They then use this colour excess to determine a star's distance and extinction.

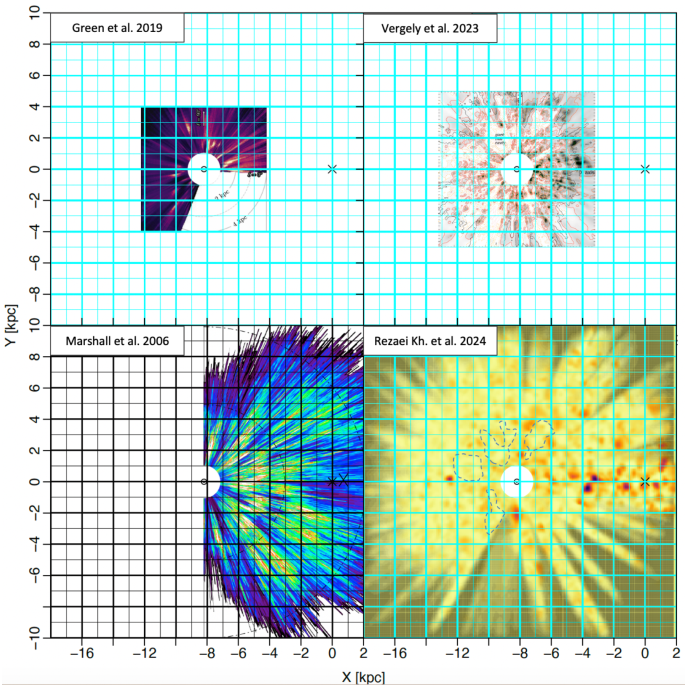

Results

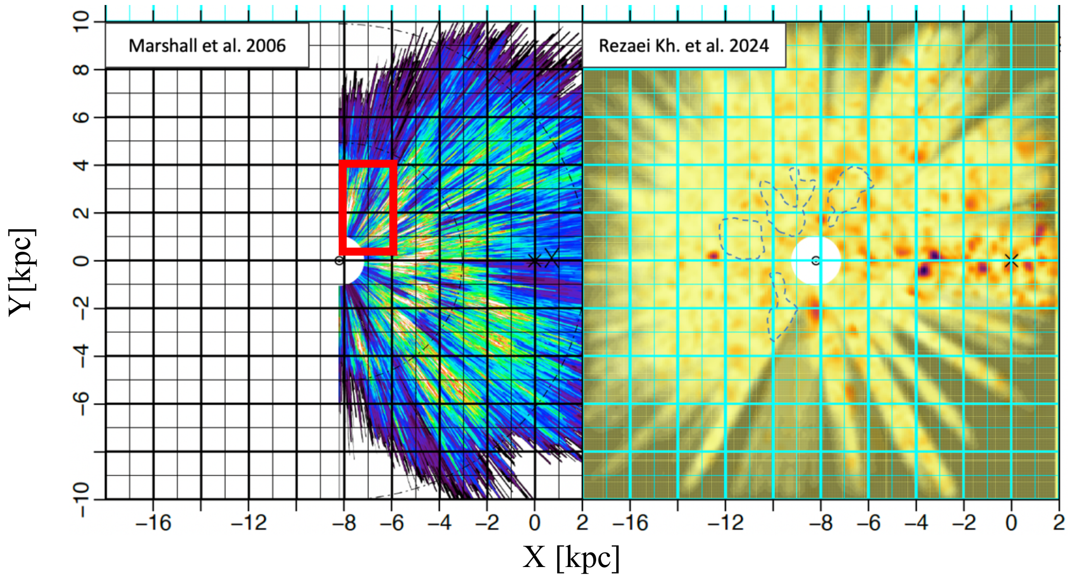

The large cavity marked in the first quadrant of our map is clearly visible in the map of Marshall et al. (2006), together with its surrounding over-densities.

While Marshall et al. (2006) reveals a cavity around and below the Galactic Centre, our map depicts a few clouds in that vicinity. Understanding the reasons for these differences presents a challenge, but we offer our insights: our input data reveals incompleteness around the Galactic Centre at b = 0.

Results

All four large cavities discovered in our map are clearly visible in Vergely et al. (2022) as well as most of their surrounding overdensities.

Differences: our map has a much larger distance coverage, and in return, the resolution of Vergely et al. (2022) is on average 4 times better than ours; as a result, they recover much smaller structures than our map can achieve.

For instance, at l = 270◦ where our map recovers a large over-density around the location of the Vela molecular cloud ((x, y) = (-8, -2) kpc), while around the same region, Vergely et al. (2022) recovers multiple smaller substructures that our map is not able to resolve.

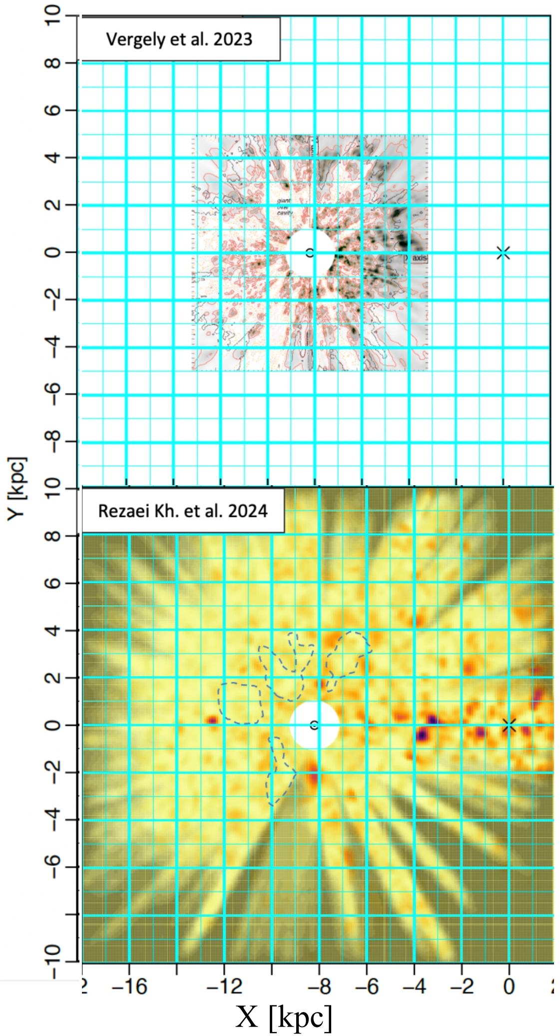

Discussion

- **4.1. Milky Way structure and masers**

We first compare our results with the locations of high-mass star-forming regions identified by trigonometric parallaxes of maser emissions (Reid et al. 2019).

There is a significant overlap between our clouds and the masers, particularly at the location of the Local arm (cyan), segments of the Perseus arm (black), as well as Sagittarius–Carina arm (purple).

Additionally, while there seems to be an offset between the masers and our clouds at the location of the Outer arm in the outer Galaxy (red points), our clouds seem to turn and follow the potential spiral arm pattern. This could suggest that the clouds and masers represent different parts of the same spiral arm.

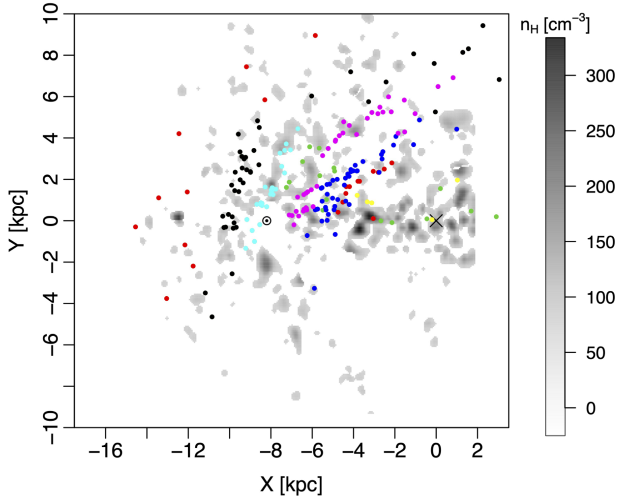

Fig. 6: Gray-scale: clouds extracted from our 3D dust map (same as Fig. 3, right). The colour coding follows the same as Fig. 1 in Reid et al. (2019). Each colour represents masers belonging to a spiral arm; 3-kpc arm: yellow – Norma–Outer arm: red – Scutum–Centaurus–OSC arm: blue – Sagittarius–Carina arm: purple – Local arm: cyan – Perseus arm: black. The Green points are equivalent to the white points in Reid et al. (2019) illustrating spurs or sources with unclear arm associations.

Discussion

- **4.2. Comparison to CO** (Miville-Deschênes et al. 2017: 8107 molecular clouds.)

There exists a good agreement between our cloud locations and the CO clouds around the position of the local arm.

Patterns on the L-V diagram typically indicative of spiral arms, and commonly used to develop and validate arm models.

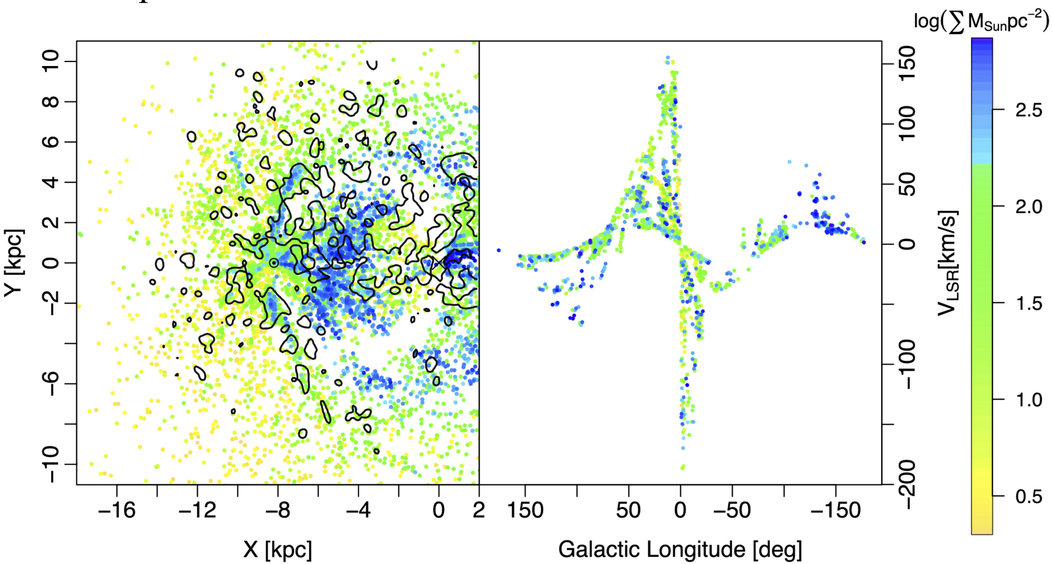

Fig. 7: Left panel: 3D distribution of the molecular clouds observed in CO from Miville-Deschênes et al. (2017), with our extracted clouds over-plotted as contours. Right panel: longitude-velocity plot of the molecular clouds from the left, situated underneath our cloud contours. The colour shows the surface density of clouds derived in Miville-Deschênes et al. (2017).

Discussion

- **4.3. Mass distribution in the Galaxy**

Overall, the total mass decreases as a function of galactocentric radius, followed by several local peaks (e.g. Elia et al. 2022; Miville Deschênes et al. 2017; Lee et al. 2016; Kennicutt & Evans 2012).

We find the first peak at about 4 kpc, likely associated with the Molecular Ring, predicted by Krumholz & McKee (2005).

The dip between 1 and 4 kpc in Miville-Deschênes et al. (2017), and similar works relying on kinematic distances, is not a real effect but rather due to lack of data in these regions.

Peak at 6.5 kpc：matches the location of the near Sagittarius–Carina arm.

Peak at 8.5 kpc: the result of the arrangement of clouds at the local arm and a large segment of the fourth quadrant.

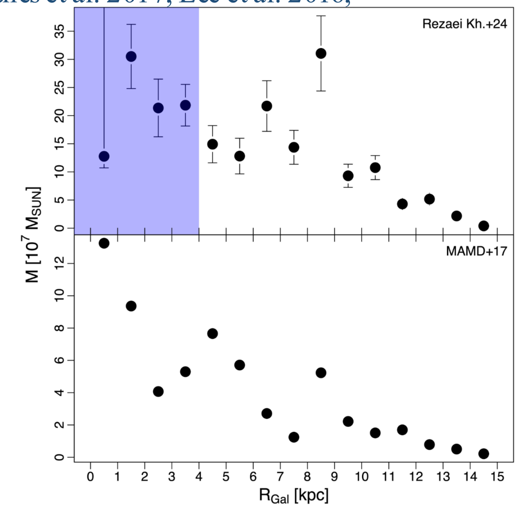

Fig. 8: Mass as a function of galactocentric Radius for clouds from our 3D map (top) and CO from Miville-Deschênes et al. (2017) (bottom) for galactocentric rings of 1 kpc thickness. In this plot, we have excluded CO clouds from Miville-Deschênes et al. (2017) belonging to regions not covered by our map (e.g. parts of the fourth quadrant). The shaded area shows regions where our results are likely underestimated due to the lack of input data. We have not limited the azimuth range for each radial bin; however, due to the limitations in the map, for regions beyond a Galactocentric radius of 2 kpc, our radial average only covers half of a circle (negative X in previous figures).

Concluding remarks

We have presented the most extended 3D dust map of the Milky Way to date and provided a catalogue of large molecular clouds in the Milky Way.

The cloud properties in the catalogue are derived from the 3D map and avoid biases involved in plane-of-the-sky works. The catalogue delivers (non-kinematic) accurate distance estimates to high-density regains and contains their volume densities. Our map illustrates large cavities in the Galactic Plane, posing as potential targets for further studies and analysis.

Our 3D map sheds light on segments of the spiral arms; however, we do not observe clear arm patterns in our results. Using the volume densities derived from our map, we also studied the distribution of mass for different Galactocentric radii. We observe an overall decreasing trend as we approach the outer Galaxy, followed by multiple local peaks linked to known regions, such as the Molecular Ring, and segments of the spiral arms.

Thank you!